

Shock-Tube Study of the Pyrolysis of the Halon Replacement Molecule $\text{CF}_3\text{CHF}\text{CF}_3$

Robert G. Hynes* and John C. Mackie

School of Chemistry, University of Sydney, NSW 2006, Australia

Assaad R. Masri

Department of Mechanical and Mechatronic Engineering, University of Sydney, NSW, 2006, Australia

Received: July 28, 1998; In Final Form: October 22, 1998

The kinetics of pyrolysis of $\text{CF}_3\text{CHF}\text{CF}_3$ have been studied in dilute mixtures (0.5 and 3 mol %) in argon in a single-pulse shock tube over the temperature range of 1200–1500 K, residence times behind the reflected shock of between 650 and 850 μs , and pressures between 16 and 18 atm. Fluorinated products were quantified with gas chromatography and Fourier transform infrared spectroscopy; identification of unknown fluorocarbons and hydrofluorocarbons was performed with gas chromatography–mass spectrometry. The most significant products detected were C_2F_6 , $\text{CF}_2=\text{CHF}$, C_2F_4 , C_3F_6 , cyclo- C_3F_6 , and $\text{CF}_3\text{CHF}\text{CF}_2\text{H}$. Traces of CF_3H , CF_4 , $\text{C}_2\text{F}_5\text{H}$, C_3F_8 , C_4F_6 , and isomers of C_4F_8 were also identified. A detailed kinetic reaction scheme is presented to model the experimental reactant and product yield profiles as a function of temperature. The results of modeling showed that the major initiation reaction was the C–C bond fission reaction. The abstraction of the secondary H atom by F atoms was also predicted to be important, whereas 1,2-HF elimination was slower. From experiments and modeling, the following initiation rate constants were obtained: $\text{CF}_3\text{CHF}\text{CF}_3 \rightarrow \text{CF}_3 + \text{CF}_3\text{CHF}$ ($k_{37} = 10^{15.9} \exp(-355.6 \text{ kJ mol}^{-1}/RT) \text{ s}^{-1}$), $\text{CF}_3\text{CHF}\text{CF}_3 \rightarrow \text{C}_3\text{F}_6 + \text{HF}$ ($k_{38} = 10^{12.9} \exp(-291.2 \text{ kJ mol}^{-1}/RT) \text{ s}^{-1}$), and $\text{CF}_3\text{CHF}\text{CF}_3 + \text{F} \rightarrow \text{CF}_3\text{CFCF}_3 + \text{HF}$ ($k_{39} = 10^{13.6} \exp(-10.1 \text{ kJ mol}^{-1}/RT) \text{ cm}^3 \text{ mol}^{-1} \text{ s}^{-1}$).

Introduction

Recent international agreements such as the Montreal Protocol and its Copenhagen Amendment have called for restrictions on the production of halons such as trifluorobromomethane (CF_3Br). This particular halon has been widely used as a fire suppressant, and its high efficiency is due to the Br atoms removing hydrogen radicals from a flame. However, CF_3Br is also responsible for severe stratospheric ozone depletion, again due to the bromine atoms. This has prompted a search for replacement fire suppressants which possess zero potential for ozone depletion yet are efficient in extinguishing a flame. Recent large-scale reviews^{1,2} have identified fluorocarbons and hydrofluorocarbons as potential halon replacements. To assist in the numerical modeling of the chemistry of potential replacement agents, a large thermochemical³ and kinetic⁴ database has been assembled. This is largely in response to the paucity of such data for fluorinated C_1 and C_2 molecules and radicals at high temperatures. However, there exists a lack of data for the three-carbon fluorocarbons, many of which are considered to be potential replacement agents.

In this work, the pyrolysis kinetics of the candidate replacement agent, 2-*H*-heptafluoropropane ($\text{CF}_3\text{CHF}\text{CF}_3$) are studied. To date, there has been no such study performed on this molecule. Only two detailed flame structure studies have been performed. Sanogo et al.⁵ have sampled low-pressure methane–oxygen–argon flames doped with 1 mol % of 2-*H*-heptafluoropropane, and Hynes et al.⁶ sampled the post-flame gases of lean, atmospheric pressure hydrogen–air flames doped with 1.0 mol % of the inhibitor. The kinetic modeling performed in both cases revealed, as expected, that the inhibitor decomposition was dominated by abstraction of the secondary hydrogen by

H, O, and OH radicals. A recent experimental study⁷ revealed that addition of large concentrations of the inhibitor (5–7 mol %; a significant fraction of the concentration required for blow-off) to near stoichiometric methane flames resulted in enhanced soot formation. This suggests that pyrolysis and other thermal decomposition reactions of the inhibitor may be of importance in suppressed flames near blow-off.

Although no previous pyrolysis studies have been performed on $\text{CF}_3\text{CHF}\text{CF}_3$, a recent study on the thermal decomposition of 2-chloro-1,1,1,2-tetrafluoroethane (CHFClCF_3)⁸ is relevant to this work. Important fluorinated (non-chlorinated) products of decomposition included C_3F_6 (major product), C_2F_4 , and isomers of perfluoro-2-butene and iso- C_4F_8 . Presented in the work of DiFelice and Ritter⁸ were QRRK analyses which indicated the importance of the singlet perfluoromethyl carbene ($^1\text{:CFCF}_3$) in the formation of C_2F_4 via 1,2-F migration isomerization and the formation of the major product, C_3F_6 .

The purpose of this work has been to study the pyrolysis of $\text{CF}_3\text{CHF}\text{CF}_3$ using the single-pulse shock-tube (SPST) technique. Gas chromatography, GC-MS, and FTIR spectrometry are used for product analysis with the aim of developing a detailed chemical kinetic mechanism to describe the decomposition of the inhibitor and the subsequent formation of products. The present study identifies important radical and carbene intermediates and provides information on their thermochemistries and reaction pathways.

Experimental Section

The shock tube used in this work has been described previously⁹ and has been used in pyrolysis studies of several hydrocarbon and organonitrogen compounds.^{10,11} Analysis of

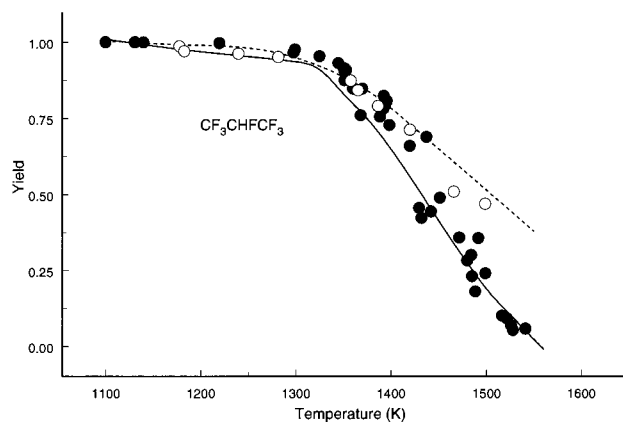


Figure 1. Variation with temperature of the CF_3CHF_3 yield: ● denotes the 0.5% mixture in Ar; ○ denotes the 3% mixture in Ar; — and --- denote model predictions for 0.5% and 3%.

the reactants and the fluorinated products was carried out with a Hewlett-Packard 6890 gas chromatograph equipped with either a HP5 or SGE-BP1 column operated at $-20\text{ }^\circ\text{C}$. Detection was by a flame ionization detector.

2-*H*-heptafluoropropane (Great Lakes) was analyzed by GC, showed no impurities, and was used without purification. In this work, the decomposition of 2-*H*-heptafluoropropane was studied in two concentration ranges: 0.5–0.6% and 3% in argon. The diluent gas was argon (99.995% minimum purity; British Oxygen Corp. Gases). A preshock GC analysis of the reactant mixture did not reveal the presence of any impurities.

The pressure and temperature behind the reflected shock were calculated from the measured incident and reflected shock velocities. Residence times were obtained from the pressure profiles recorded using Kistler pressure transducers. The experiments were performed over the temperature range 1200–1550 K for low concentration runs and 1200–1500 K for the higher concentration runs. This upper temperature limit was set in the higher concentration runs by the onset of formation of high molecular weight compounds. Typical residence times behind the reflected shocks were 650–850 μs with pressures between 16 and 18 atm. Product identification was performed with a Hewlett-Packard 5890 II GC interfaced with a Hewlett-Packard 5898A MS Engine.

Calibration of fluorinated hydrocarbons was performed daily with a dilute mixture of CF_3H (Sigma-Aldrich; 98+% purity), C_2F_6 (Sigma-Aldrich; 98+% purity), C_3F_6 (Matheson; 99.5+% purity), and CF_3CHF_3 in argon. The responses for C_3F_6 and CF_3CHF_3 were nearly identical. The FID responses of products such as C_2F_4 and $\text{CF}_2=\text{CFH}$, for which calibration samples were not available, were assumed to be 0.667 of the response of the C_3 fluorocarbons on a molar basis. Trace products such as CF_4 which did not undergo chemionization in the FID were determined by FTIR.

Results and Discussion

Carbon mass balances of reactants and recovered products were generally of the order of $100 \pm 10\%$ at temperatures of $\leq 1500\text{ K}$ for the lower concentration runs and $\leq 1450\text{ K}$ for the higher concentration runs. At higher temperatures, the carbon recovery dropped to 80%, suggesting the formation of higher molecular weight fluorocarbons and perhaps polymeric species, although these were not detected.

An analysis of the FTIR spectra did not reveal traces of CO , CO_2 , or CF_2O , hence impurities by oxygen were not considered to be important in these experiments.

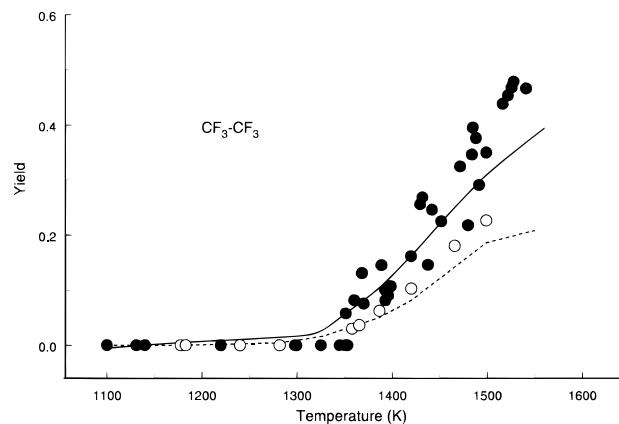


Figure 2. Variation with temperature of the CF_3-CF_3 yield: ● denotes the 0.5% mixture in Ar; ○ denotes the 3% mixture in Ar; — and --- denote model predictions for 0.5% and 3%.

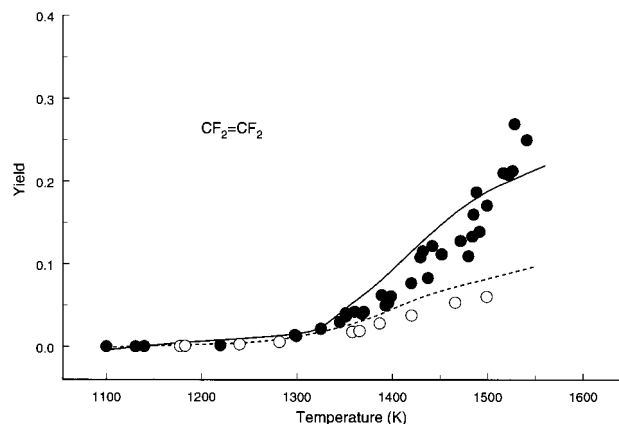


Figure 3. Variation with temperature of the $\text{CF}_2=\text{CF}_2$ yield: ● denotes the 0.5% mixture in Ar; ○ denotes the 3% mixture in Ar; — and --- denote model predictions for 0.5% and 3%.

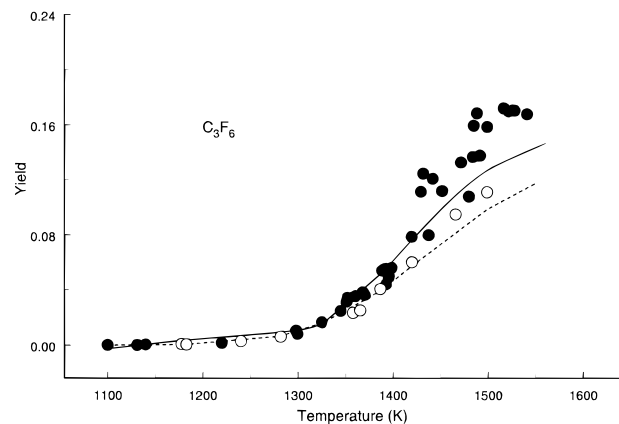


Figure 4. Variation with temperature of the C_3F_6 yield: ● denotes the 0.5% mixture in Ar; ○ denotes the 3% mixture in Ar; — and --- denote model predictions for 0.5% and 3%.

Figures 1–7 show profiles of the yield versus the frozen reflected shocked gas temperature for all products of significance in the pyrolysis of CF_3CHF_3 (with the exception of HF , which could not be measured due to its reactivity with the walls of the product vessel). At both low and high initial concentrations, the inhibitor began to decompose at a temperature of 1320 K. At the lowest temperatures at which decomposition occurred, traces of C_2F_4 and C_3F_6 were detected. At $\sim 1370\text{ K}$, C_2F_6 began to form, and this became the dominant product at increasingly higher temperatures. At 1450 K, approximately 25% of the

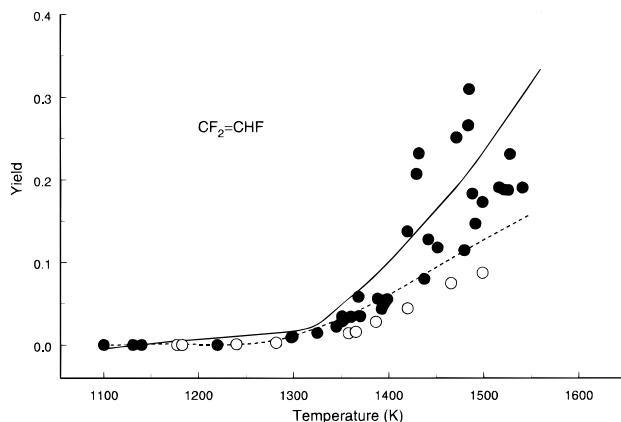


Figure 5. Variation with temperature of the $\text{CF}_2=\text{CHF}$ yield: ● denotes the 0.5% mixture in Ar; ○ denotes the 3% mixture in Ar; — and --- denote model predictions for 0.5% and 3%.

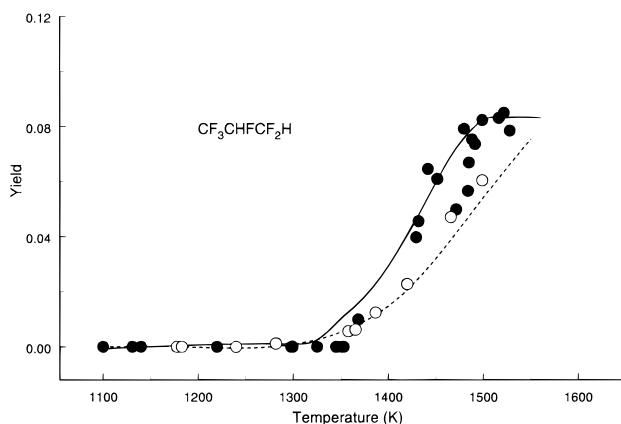


Figure 6. Variation with temperature of the $\text{CF}_3\text{CHFCF}_2\text{H}$ yield: ● denotes the 0.5% mixture in Ar; ○ denotes the 3% mixture in Ar; — and --- denote model predictions for 0.5% and 3%.

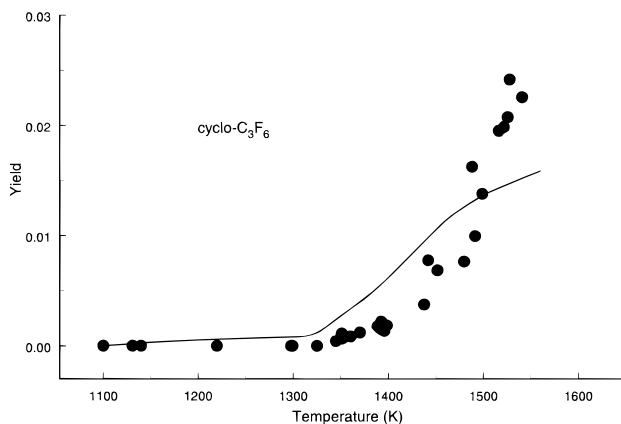


Figure 7. Variation with temperature of the cyclo- C_3F_6 yield: ● denotes the 0.5% mixture in Ar; — denotes model prediction for 0.5%.

product yield was C_2F_6 and $\sim 12\%$ was C_3F_6 . Also important was the compound $\text{CF}_2=\text{CHF}$ whose product yields were slightly higher than those obtained for C_3F_6 at temperatures above 1400 K. In lesser quantities were the $\text{CF}_3\text{CHFCF}_2\text{H}$ and cyclo- C_3F_6 species. Minor products included CF_3H in maximum yields of 5% and CF_4 whose yield was less than 2% (the CF_4 was present only in runs above 1550 K). Other trace products included C_3F_8 , $\text{CF}_3\text{CF}_2\text{H}$, iso- C_4F_8 , C_4F_6 (identified as perfluoro-2-butyne by GC-MS), as well as heavier cyclic compounds. For the same frozen gas temperatures behind the reflected shock, it can be seen that the reactant decomposition is lower in the higher

concentration runs. This can arise partly through a dependence of reaction order other than first order in the initial reactant concentration or through the significant decrease in temperature with reaction behind the reflected shock in the case of the 3% mixture. The yields of C_2F_4 and $\text{CF}_2=\text{CHF}$ also depend on the initial concentration, whereas the formation of C_3F_6 , $\text{CF}_3\text{-CHFCF}_2\text{H}$, and C_2F_6 were found to be largely invariant to the initial reactant concentration.

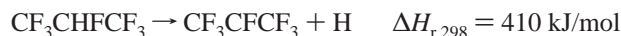
The Reaction Model

A 68-step reaction model was developed in this work to describe the decomposition of $\text{CF}_3\text{CHFCF}_3$, as summarized in Table 1. It should be noted that the reverse Arrhenius parameters are fitted with a T^0 dependence in order to verify the accuracy of the thermochemical data used. In the actual numerical modeling (see the Kinetic Modeling section below), the reverse rate parameters are computed from the equilibrium constant at each temperature; temperature dependences in the A -factor are included.

To model the temperature variation of the product yields it is first necessary to discuss the probable initiation reactions. The observation of C_3F_6 at low temperatures was indicative of a unimolecular 1,2-elimination of HF. The formation of C_2F_6 at higher temperatures also suggests that C–C single bond fission is occurring to form CF_3 which subsequently recombine. Both initiation reactions (reactions 38 and 37 from Table 1) are given below



C–H bond fission is also possible, yielding the CF_3CFCF_3 radical



This pathway is expected to be less important than the C–C rupture because the bond enthalpy is higher by 43 kJ/mol and a hydrogen atom, rather than a heavy CF_3 group, is lost in the C–H fission, resulting in a lower A -factor. A more facile route to H loss is via F and CF_3 radical abstraction to form the $\text{CF}_3\text{-CFCF}_3$ radical (reactions 41 and 39).

An important part of the reaction mechanism involves the CF_3CHF radical produced by C–C bond fission. No experimental thermochemistry is available for this radical. Ab initio calculations were first performed by Chen et al.¹² using low-level UHF/6-31G* theory. The $\Delta H_{f,298}^\circ$ calculated at this level of theory was -688.3 kJ/mol. A subsequent higher level BAC-MP4 calculation³ gave $\Delta H_{f,298}^\circ = -703.0$ kJ/mol, and a recent G2 calculation¹³ based on isodesmic reactions gave a result of -690.8 ± 4.2 kJ/mol. The value of Chen *et al.*¹² was adopted in this work. A feasible route for destruction of this radical is by loss of a fluorine atom from the CF_3 group to form the stable 1,1,2-trifluoroethene, which is observed as a major product (reaction 27)




Reaction 27 is also expected to be a major production route for F atoms. Because the C–C bond enthalpy is 350 kJ/mol, the alternative bond scission route (reaction 28) is less favorable. Also observed in the product mixture is the $\text{CF}_3\text{CHFCF}_2\text{H}$ molecule, which could result from the recombination of $\text{CF}_3\text{-CHF}$ and CF_2H radicals. The CHF_2 may also recombine with CF_3 giving $\text{CF}_3\text{CF}_2\text{H}$. However the large yield of C_2F_6 and the

TABLE 1: Reaction Model for CF₃CHF₂CF₃ Pyrolysis^a

	reactions	forward reaction			reverse reaction			ref
		log A	<i>n</i>	<i>E</i>	log A	<i>n</i>	<i>E</i>	
1	F ₂ + M = 2F + M	10.1	0.77	117.2	11.7	0	-28.1	24
2	2H + M = H ₂ + M	18.0	-1	0.0	15.0	0	425.3	4
3	HF + M = H + F + M	13.5	0	415.6	12.7	0	-155.8	4
4	H ₂ + F = H + HF	12.4	0.5	2.7	14.3	0	142.9	4
5	CF ₃ + F = CF ₄	38.2	-7.9	37.4	13.0	0	480.0	4
6	CF ₂ + F = CF ₃	12.9	0	0.0	14.7	0	349.8	4
7	2CF ₃ = CF ₃ -CF ₃	13.5	0	0.0	17.3	0	381.8	14
8	CHF ₃ = CF ₂ + HF	14.1	0	302.1	11.4	0	77.3	25
9	CF ₃ + CF ₂ = CF ₃ -CF ₂	13.0	0	0.0	15.4	0	214.5	estd
10	CH ₂ F-CF ₃ = CH ₂ F + CF ₃	17.0	0	373.6	13.6	0	-0.3	estd
11	CH ₂ F-CF ₃ = HF + CHF:CF ₂	13.4	0	296.2	11.2	0	180.3	4
12	2CH ₂ F = CH ₂ F-CH ₂ F	13.5	0	0.0	17.3	0	351.4	estd
13	2CHF ₂ = CHF ₂ -CHF ₂	13.5	0	0.0	17.3	0	361.2	estd
14	CHF ₃ + F = CF ₃ + HF	13.7	0	15.5	12.7	0	140.5	4
15	CF ₃ CF + CHF = C ₃ F ₅ H	12.9	0	0.0	15.6	0	482.0	estd
16	CF ₃ -CF ₂ = CF ₂ :CF ₂ + F	14.7	0	334.7	13.8	0	32.5	estd
17	CF ₂ :CF ₂ + F = CF ₃ + CF ₂	13.5	0	0.0	12.0	0	87.7	estd
18	CF ₂ :CF ₂ = 2CF ₂	16.7	0	292.9	13.5	0	30.8	26
19	CF ₂ :CF + F = 2CF ₂	13.3	0	0.0	13.2	0	249.7	estd
20	CF ₂ :CF + H = CHF:CF ₂	34.4	-7.1	21.1	10.6	0	429.4	4
21	CHF:CF ₂ = C ₂ F ₂ + HF	14.4	0	418.4	13.1	0	190.2	4
22	F + CHF:CF ₂ = CHF ₂ -CF ₂	50.7	-11.1	75.7	12.1	0	190.7	QRRK
23	F + CHF:CF ₂ = CHF ₂ + CF ₂	26.0	-3.32	37.7	12.6	0	33.8	QRRK
24	CHF ₂ -CF ₂ = CHF ₂ + CF ₂	15.0	0	225.9	12.4	0	16.9	estd
25	F + CHF:CF ₂ = CF ₂ :CF + HF	13.0	0	20.9	12.0	0	101.2	estd
26	CHF + CF ₂ = CHF:CF ₂	13.0	0	11.8	15.9	0	426.7	4/PW
27	CF ₃ -CHF = F + CHF:CF ₂	14.8	0	259.4	13.3	0	2.2	PW
28	CF ₃ -CHF = CF ₃ + CHF	16.0	0	349.4	13.4	0	27.2	estd
29	CF ₃ -CHF + F = CHF ₂ -CF ₃	13.5	0	0.0	15.7	0	492.6	estd
30	CF ₃ -CHF + F = CF ₃ CF + HF	13.7	0	0.0	13.2	0	264.5	estd
31	CF ₃ -CHF + H = CF ₃ CF + H ₂	13.7	0	0.0	13.1	0	130.1	estd
32	CHF ₂ -CF ₃ = CF ₃ + CHF ₂	17.0	0	388.3	13.6	0	23.2	estd
33	CF ₃ -CHF = CF ₃ CF + H	14.7	0	312.5	13.5	0	5.7	estd
34	CF ₃ -CHF = CF ₂ :CF + HF	14.0	0	313.8	11.4	0	136.9	estd
35	CF ₃ -CHF + CF ₃ = CF ₃ CF + CHF ₃	12.7	0	8.4	13.2	0	147.9	estd
36	C ₃ F ₇ H = <i>i</i> -C ₃ F ₇ + H	14.8	0	410.0	14.2	0	3.3	estd
37	C ₃ F ₇ H = CF ₃ + CF ₃ -CHF	15.9	0	355.6	13.4	0	0.7	PW
38	C ₃ F ₇ H = C ₃ F ₆ + HF	12.9	0	291.2	10.6	0	178.8	PW
39	C ₃ F ₇ H + F = <i>i</i> -C ₃ F ₇ + HF	13.6	0	10.0	13.8	0	174.6	PW
40	C ₃ F ₇ H + H = <i>i</i> -C ₃ F ₇ + H ₂	7.1	1.6	42.7	13.0	0	91.5	4
41	C ₃ F ₇ H + CF ₃ = <i>i</i> -C ₃ F ₇ + CHF ₃	11.0	0	42.7	12.1	0	82.3	4
42	<i>i</i> -C ₃ F ₇ = CF ₃ CF + CF ₃	15.8	0	255.2	12.7	0	0.2	PW
43	<i>i</i> -C ₃ F ₇ = C ₃ F ₆ + F	14.3	0	301.2	11.8	0	24.2	PW
44	<i>i</i> -C ₃ F ₇ + CF ₃ -CHF = C ₃ F ₇ H + CF ₃ CF	13.5	0	20.9	12.9	0	120.9	estd
45	C ₃ F ₆ = CF ₃ CF + CF ₂	13.0	0	328.0	10.6	0	0.2	PW
46	CF ₃ CF = CF ₂ :CF ₂	11.5	0	167.4	12.4	0	237.8	8
47	C ₃ F ₆ = CF ₂ :CF + CF ₃	16.7	0	439.3	13.9	0	19.9	PW
48	CF ₃ CHFCF ₂ H = CF ₃ -CHF + CHF ₂	16.0	0	372.4				estd
49	CF ₃ -CHF + CHF ₂ = CF ₃ CHFCF ₂ H	13.7	0	0.0				estd
50	CF ₂ :CF ₂ + CF ₂ = cyclo-C ₃ F ₆	11.3	0.5	35.6				17
51	cyclo-C ₃ F ₆ = CF ₂ :CF ₂ + CF ₂	13.0	0	182.0				17
52	C ₃ F ₆ + F = CF ₃ -CF ₂ + CF ₂	51.7	-10.9	177.2	11.9	0	95.0	QRRK
53	C ₃ F ₆ + F = CF ₂ :CF ₂ + CF ₃	49.8	-10.8	157.9	11.3	0	124.6	QRRK
54	CF ₃ -CF ₂ + CF ₂ = <i>n</i> -C ₃ F ₇	12.6	0	8.4	14.8	0	205.6	26
55	<i>n</i> -C ₃ F ₇ = CF ₂ :CF ₂ + CF ₃	14.0	0	190.0	12.6	0	40.3	26
56	C ₃ F ₈ = CF ₃ -CF ₂ + CF ₃	17.0	0	374.5	13.1	0	0.0	estd
57	2CF ₃ CF = <i>t</i> -C ₄ F ₈	12.8	0	8.4	15.6	0	411.0	estd
58	C ₃ F ₆ + CF ₂ = <i>i</i> -C ₄ F ₈	13.6	0	154.3	17.5	0	422.6	estd
59	2 CF ₂ :CF ₂ = C ₃ F ₆ + CF ₂	12.0	0	125.5	10.3	0	120.9	27
60	<i>c</i> -C ₄ F ₈ → 2CF ₂ :CF ₂	16.0	0	310.9				28
61	2CF ₂ :CF ₂ → <i>c</i> -C ₄ F ₈	11.7	0	100.4				PW/29
62	2CF ₂ :CF = C ₄ F ₆	12.5	0	0.0	17.5	0	551.5	estd
63	CF ₃ + <i>i</i> -C ₃ F ₇ → <i>i</i> -C ₄ F ₁₀	13.7	0	0.0				estd
64	<i>i</i> -C ₄ F ₁₀ → CF ₃ + <i>i</i> -C ₃ F ₇	16.0	0	376.6				estd
65	C ₃ F ₆ + CF ₃ → <i>i</i> -C ₄ F ₉	11.7	0	33.5				estd
66	<i>i</i> -C ₄ F ₉ → C ₃ F ₆ + CF ₃	12.8	0	150.6				estd
67	<i>i</i> -C ₄ F ₉ → <i>i</i> -C ₄ F ₈ + F	14.0	0	225.9				estd
68	<i>i</i> -C ₄ F ₈ + F → <i>i</i> -C ₄ F ₉	13.0	0	4.2				estd

^a Units for A: cm³ mol⁻¹ s⁻¹ or s⁻¹ as appropriate. Units for *E*: kJ/mol. PW indicates rate coefficient evaluated in the present work. estd indicates rate coefficient was estimated in the present work. QRRK: rate coefficients estimated by quantum RRK methods in the present work.

TABLE 2: Thermochemical Parameters for the CF₃CHF₂CF₃ System

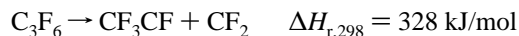
structure	name ^a	$\Delta H_{f,298}^{\circ}$ kJ/mol	S_{298}° J/K-mol	C_p° J/K-mol					ref
				300	500	1000	1500	2000	
CF ₃ CHF ₂ CF ₃	C ₃ F ₇ H	-1528	413.4	136.0	132.1	226.8	238.3	243.6	6
CF ₃ ĊFCF ₃	<i>i</i> -C ₃ F ₇	-1335	402.1	129.7	169.8	211.7	224.6	230.1	6
CF ₃ CF=CF ₂	<i>c</i> -C ₃ F ₆	-1125	395.8	124.5	155.0	186.1	195.3	198.8	6
CF ₃ CHF ₂ CF ₂ H	CF ₃ CHF ₂ CF ₂ H	-1294	396.6					-	30
CF ₃ CF:	CF ₃ CF:	-586	321.4	77.2	98.7	118.8	124.1	126.1	PW
	cyclo-C ₃ F ₆	-979	342.7	110.8	159.8	201.7	204.1	204.8	31
CF ₃ -ĊHF	CF ₃ -CHF	-688	318.8	85.5	110.7	136.3	144.5	147.8	12/PW
CHF ₂	CHF ₂	-248	255.9	42.3	54.1	69.6	75.6	78.3	32,4
CF ₃	CF ₃	-467	265.2	50.0	63.3	76.9	79.8	81.3	32,4

^a Name as shown in Table 1.

trace amounts of CF₃CF₂H suggest that this is not a competitive route. Large yields of the CF₃CHF radical are expected from the C–C rupture, as evidenced by the yields of CF₂=CHF. Termination of F atoms with CF₂=CHF should, therefore, be important due to the large concentration of each species. Termination of F atoms by CF₃CF₂CF₃ also occurs, but this route is not competitive due to the low yields of C₃F₈. For the same reason, F termination by reactions with C₃F₆ and C₂F₄ are also not competitive. F addition to CF₂=CHF produces (reaction 23) CF₂H and CF₂. These products can also form by the C–C bond fission of the chemically activated CF₂-CHF₂* intermediate (reactions 22 and 24). The recombination of CF₂H and CF₃-CHF yields a thermodynamically stable product, with an enthalpy of formation of -1294 kJ/mol, making this recombination route plausible.

The product in largest yield was C₂F₆, which was formed primarily by the recombination of CF₃ radicals (reaction 7). The rate constant used in the kinetic model (reaction 7) for the recombination was that derived by Glänzer et al.¹⁵ for the pressure range from 0.3 to 25 atm at 1300 K.

Another important product is C₂F₄, which can arise from two sources: C₃F₆ and the CF₃CF₂CF₃ radical. The latter species is formed via abstraction reactions with F and CF₃ (reactions 39 and 41). The first process involves breaking the double bond to form CF₂ and the singlet CF₃CF: carbene (reaction 45)



Thermochemically, however, the single bond breakage in CF₃-CF₂CF₃ appears to be the more favorable route (reaction 42)



Although CF₃CHF formed in the initiation step could also undergo C–H bond scission (reaction 33) to form the carbene, the high bond enthalpy (320 kJ/mol) makes this route much less likely.

The CF₃CF: so formed is an important precursor of C₂F₄. To date there exists a paucity of reliable experimental information on the 1,2-F migration isomerization kinetics of this carbene. The $\Delta H_{f,298}^{\circ}$ was estimated to be -586 kJ/mol, which is in good agreement with the $\Delta H_{r,298}^{\circ}$ for the isomerization reaction (-75.3 kJ/mol) estimated by DiFelice and Ritter.⁸ The

exothermicity of the reaction suggests its importance (reaction 46)



Given the importance of the carbene and the lack of experimental thermochemical or kinetic data, ab initio calculations have been employed to derive the various quantities. Energies and geometries for the singlet carbene have been calculated by Dixon¹⁵ using a double- ζ basis set with polarization functions on the C atoms. O'Gara and Dailey¹⁶ have also calculated geometries as well as energies and harmonic frequencies using a variety of methods. Recently,¹³ these quantities were calculated with HF/6-31G(d) theory and were used to calculate the entropies and heat capacities of the carbene using statistical thermodynamics. The derived thermochemical quantities are shown in Table 2. The preexponential factor for the 1,2-F migration in the carbene was optimized in the present model and is in good agreement with that proposed by DiFelice and Ritter.⁸ The barrier for the isomerization used in this work is 167 kJ/mol, based on a G2-MP2 calculation.¹³ This is again in reasonable agreement with a previous value for the barrier⁸ of 151 kJ/mol.

It has been suggested⁸ that the triplet CF₃CF: might also be important in the pyrolysis since it lies only 38 kJ/mol above the singlet state.¹⁵ In this model, however, only the singlet state has been considered.

Observed in small quantities was cyclo-C₃F₆, which formed from the addition of singlet CF₂ to C₂F₄. The barriers for formation and destruction of this species adopted in this work are similar to that proposed by Atkinson and McKeegan,¹⁷ although their experiments were conducted at lower temperatures and pressures than those used in this work. The A-factor for the formation was increased by an order of magnitude in order to correctly model the yields.

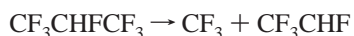
The model shown in Table 1 also includes pathways for the formation of heavier C₃ and C₄ compounds including C₃F₈, C₄F₆, and isomers of C₄F₈. Product yields of these species were less than 1–2% and could not be accurately modeled. The addition compound iso-C₄F₁₀ was also included but was not detected in these experiments.

Kinetic Modeling

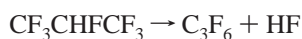
Kinetic modeling of the detailed reaction mechanism given in Table 1 was performed with the Sandia code CHEMKIN¹⁸ together with a shock-tube code¹⁹ modified to include the effects of quenching by the reflected rarefaction wave and the LSODE ordinary differential equation solver.²⁰ The code SENKIN²¹ was used for sensitivity analyses.

In Figures 1–7, the experimental product and reactant decomposition profiles are compared with those predicted by the model. The predicted profiles for the major products at both concentrations lie within experimental error. The minor product cyclo-C₃F₆ is also predicted in reasonable agreement with experiment.

The major initiation reactions in the model include reactions 37–39 and 41. The rate constants for these reactions that best fit the experimental yield profiles are



$$k_{37} = 10^{15.9} \exp(-355.6/RT) \text{ s}^{-1}$$

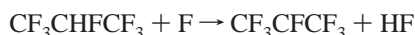


$$k_{38} = 10^{12.9} \exp(-291.2/RT) \text{ s}^{-1}$$

where the activation energies are in kJ/mol.

The Arrhenius parameters optimized for these initiation steps have *A* factors in the expected range for a loose transition state (*A*₃₇) and for a tight, four-center transition state (*A*₃₈). The optimized activation energy for the C–C breakage, *E*₃₇, is 1 kJ/mol less than the bond enthalpy over the temperature and pressure range of 1000–2000 K and 16–18 atm. *E*₃₈ is derived from the heat of reaction with an additional barrier of 162 kJ/mol for the formation of the four-center transition state, which is typical of 1,2-HF elimination reactions in hydrofluorocarbon molecules.⁴ At a total pressure of 16–18 atm, these reactions should be at or near the high-pressure limit.

The rate constants for the abstraction of the secondary hydrogen atom by F and CF₃ have been estimated from the analogous reactions of two-carbon hydrofluorocarbons.⁴ The most important of these routes is the F-atom abstraction by virtue of its higher *A*-factor and lower barrier



$$k_{39} = 10^{13.6} \exp(-10.1/RT) \text{ cm}^3 \text{ mol}^{-1} \text{ s}^{-1}$$

A sensitive reaction in the model is the loss of F from the CF₃CHF radical (reaction 27). Since no analogous fluorinated system could be found, the *A*-factor was set to a value typical of a C–H bond scission from C₂H₅, then optimized to give the correct product yields. The value of *E*₂₇ was 260 kJ/mol between 1000 and 2000 K. This value differs from the C–F bond enthalpy at these temperatures by only 2 kJ/mol.

The thermochemical database used in the modeling is based on the work of Burgess et al.⁴ with the exception of those species so indicated in Table 2. The heat of formation of the carbene, :CHF, derived by Pritchard et al.²² was found to be too high ($\Delta H_{f,298}^\circ$ (:CHF) = 163 kJ/mol). This value led to incorrect reverse activation barriers for reactions involving this species (particularly reaction 28). The value derived by Pritchard et al.²² is based on low-level UHF/4-31G calculations at the optimized STO-3G geometry. The calculations were based on only four isodesmic reactions for which uncertain heats of formation were used. Instead, the heat of formation derived by Zachariah et al.³ using the BAC-MP4 method, which gave $\Delta H_{f,298}^\circ$ (:CHF) = 131.7 kJ/mol, was used. This provided a

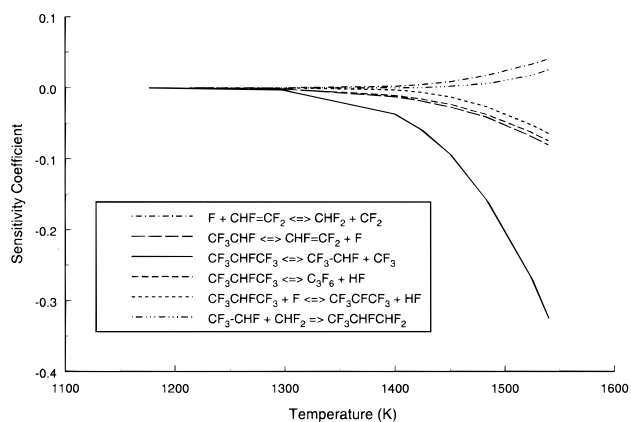


Figure 8. Variation with temperature of the sensitivity coefficients for the reactant CF₃CHFCF₃.

more accurate reverse barrier for reaction 28. This value of Zachariah et al.³ is in good agreement with a recent G2 calculation by Poutsma et al.²³ of $\Delta H_{f,298}^\circ$ (:CHF) = 132.6 kJ/mol. The deviation from their experimental result was 12 kJ/mol.

The inadequacy of other thermochemical data required certain reactions to be decoupled into pairs of irreversible reactions. This involved the cyclo-C₃F₆ and CF₃CHFCF₂H species (reactions 45–46 and 50–51). The rate coefficients were then individually optimized to give correct product yields. Reactions for *i*-C₄F₁₀ were also decoupled in a similar way, although this species is insignificant in this work.

Sensitivity and Rate of Production Analyses

The sensitivity data for decomposition of 0.5 mol % CF₃CHFCF₃ are shown in Figure 8. Clearly, the most sensitive reaction at all temperatures is the C–C unimolecular bond fission in CF₃CHFCF₃. The sensitivity of the 1,2-elimination of HF from the reactant is lower by a factor of 3. Of equal sensitivity to this reaction was the F loss from the CF₃CHF radical. Of the abstraction reactions, the only sensitive reaction was the F abstraction of the secondary hydrogen atom to form HF. Two reactions showed positive sensitivity coefficients (i.e., formation of the reactant) at temperatures ≥ 1400 K: F addition to CHF=CF₂ and formation of CF₃CHFCF₂H by recombination of CF₃CHF and CF₂H (reaction 49). The depletion of F atoms from the radical pool by reaction 23 prevents them from abstracting the secondary hydrogen from the reactant, thus explaining its positive sensitivity coefficient. The removal of CHF₂ in reaction 49 causes reaction 23 to consume more F atoms.

Figure 9 displays a summary of the reaction fluxes important in the decomposition of the reactant and the formation of products for an initial reactant concentration of 0.5% and a frozen reflected shocked gas temperature of 1500 K. The flux analysis shows that the C–C fission (reaction 37) accounts for 60.5% consumption of the reactant; the 1,2-elimination channel accounts for 11%. The lower flux through reaction 38 is probably due to its lower *A*-factor. The abstraction route, reaction 39, however, accounts for 17.3% of the reactant destruction, whereas abstraction by CF₃ accounts for only 0.5%. Interestingly, the reverse of reaction of 37 accounts for 11% production of CF₃CHFCF₃.

The flux analysis for 3% reactant is somewhat ambiguous because of the rapid and significant cooling that occurs after the passage of the reflected shock. After 100 μ s, the flux analysis shows that the mixture has cooled from 1500 to 1450 K. As

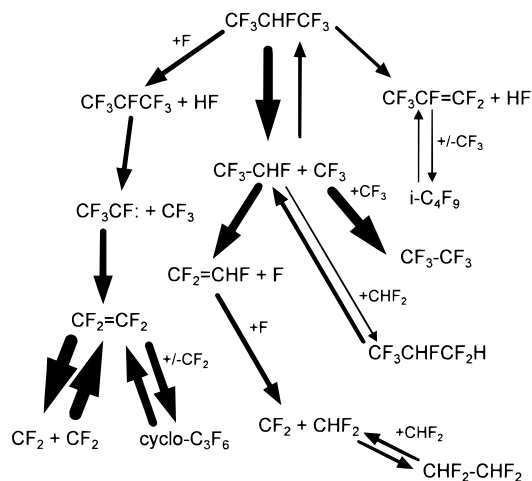


Figure 9. Reaction fluxes for CF_3CHF_3 decomposition and product formation. The largest arrows indicate the reactions with the largest flux. The conditions are 0.5% initial reactant concentration and a temperature of 1500 K.

noted above, the reformation of the reactant is also significant and further enhances the heat capacity of the product mixture.

Sensitivity analysis also shows that the major products C_2F_6 , C_2F_4 , and $\text{CF}_2=\text{CHF}$ are very sensitive to reactions 37 and 27 at temperatures above 1400 K. The product C_3F_6 is sensitive to reaction 38 as expected and also to the two abovementioned reactions.

As noted above, the production of F atoms is important in this model. The principal source of F is from the CF_3CHF radical (44%). As noted above, reactions 39 and 23 account for 18% and 23% of the F destruction routes, respectively.

Discussion

In terms of flame chemistry, this study is most relevant to fuel-rich flames with a high CF_3CHF_3 loading. In rich, uninhibited flames, the fuel competes with O_2 for H radicals; this behavior is self-inhibitory, as described by Linteris et al.⁷ The higher concentration of CH_3 radicals in these fuel-rich flames gives rise to higher rates of chain termination, leading to the formation of C_2H_6 and C_2H_4 . Addition of inhibitor to these flames provides more competition for H but at the same time it is expected that pyrolysis of the inhibitor will occur given the lower radical concentrations. As suggested by Linteris et al.,⁷ the initiation step at lower loadings in fuel-rich flames should proceed by abstraction of the secondary H atom^{5,6} by CH_3 and other radicals to form CF_3CFCF_3 . At higher loadings, the same initiation step will take place, however, the 1,2-HF elimination reaction forming $\text{CF}_3\text{CF}=\text{CF}_2$ and C–C bond rupture will also occur. The formation of unsaturated fluorocarbon compounds observed in this study can undergo addition reactions with CH_3 and other radicals, forming larger fluorinated species or soot precursors. In fact, most of the two- and three-carbon products observed in the pyrolysis study have also been observed in laminar counterflow CH_4 -diffusion flames inhibited with CF_3CHF_3 :³³ $\text{CF}_3\text{-CF}_3$, $\text{CF}_2=\text{CF}_2$, $\text{CF}_3\text{CF}=\text{CF}_2$, and $\text{CHF}=\text{CF}_2$. Also observed was $\text{CF}_2=\text{CH}_2$ and heavier species including hexafluorobutene, benzene, fluorobenzene, 1,2-difluorobenzene, trifluoromethylbenzene, and toluene. This indicates that the chemistry of inhibitor consumption in rich environments is quite different to that observed in fuel-lean environments, where partially oxidized species including CF_2O and CF_3CFO ⁶ were observed at 1.0% loading. At a higher loading of 3.2% in lean flames, the temperature of the flame

increased but the mode of inhibitor decomposition was found to be similar to that observed at the 1.0% loading. Clearly, the chemical kinetics of inhibitor destruction in rich flames are not well understood and need to be studied in more depth.

Conclusion

Inspection of the product yields and reaction-path analysis suggests that CF_3CHF_3 decomposes primarily by C–C bond fission at temperatures above 1300 K, pressures between 16 and 18 atm, and residence times of 650–850 μs . Reaction-path analysis also shows that the abstraction of the secondary H atom by F was found to be the next most important destruction route, whereas the 1,2-HF elimination channel was found to be slower. Kinetic modeling showed that the fate of the CF_3 radicals produced in the major initiating reaction was recombination to form C_2F_6 ; only traces of CF_3H and CF_4 were observed. The fate of the CF_3CHF radicals was loss of an F atom from the CF_3 group to form the stable $\text{CF}_2=\text{CHF}$ molecule. Formation of C_2F_4 proceeds from the CF_3CFCF_3 radical which undergoes C–C bond scission to form the carbene, $\text{CF}_3\text{CF:}$. This undergoes a 1,2-F-shift isomerization reaction to form the product.

The yields of all major and minor products have been satisfactorily described by the detailed kinetic model involving the aforementioned radicals. For 3% reactant, product yields of CF_3CHF_3 were lower, suggesting either a non-first-order dependence of the reactant decomposition rate on the reactant concentration or the rapid reactive cooling that takes place behind the reflected shock at this high reactant concentration.

Acknowledgment. We thank Dr. G. B. Bacskay and Mr. M. Smith for performing the G2-MP2 calculations used in this work.

References and Notes

- (1) Nyden, M. D.; Linteris, G. T.; Burgess, D. R., Jr.; Westmoreland, P. R.; Tsang, W.; Zachariah, M. R. *Flame Inhibition Chemistry and the Search for Additional Fire Fighting Chemicals*. In *Evaluation of Alternative In-Flight Fire Suppressants for Full-Scale Testing in Simulated Aircraft Engine Nacelles and Dry Bays*; Grosshandler, W., Gann, R., Pitts, W., Eds.; NIST Spec. Pub. 861; National Institute of Standards and Technology: Gaithersburg, MD, 1994; pp 467–641.
- (2) *Halon Replacements: Technology and Science*; Miziolek, A., Tsang, W., Eds.; ACS Symposium Series; American Chemical Society: Washington, DC, 1995; Vol. 611.
- (3) Zachariah, M. R.; Westmoreland, P. R.; Burgess, D. R., Jr.; Tsang, W.; Melius, C. F. *J. Phys. Chem.* **1996**, *100*, 8737.
- (4) Burgess, D. R., Jr.; Zachariah, M. R.; Tsang, W.; Westmoreland, P. R. *Prog. Energy Combust. Sci.* **1996**, *21*, 453.
- (5) Sanogo, O.; Delfau, J.-L.; Akrieh, R.; Vovelle, C. *Combust. Sci. Technol.* **1997**, *122*, 33.
- (6) Hynes, R. G.; Mackie, J. C.; Masri, A. R. *Combust. Flame* **1998**, *113*, 554.
- (7) Linteris, G. T.; Burgess, D. R., Jr.; Babushok, V.; Zachariah, M.; Tsang, W.; Westmoreland, P. *Combust. Flame* **1998**, *113*, 164.
- (8) DiFelice, J.; Ritter, E. R. *Combust. Sci. Technol.* **1996**, *116–117*, 5.
- (9) Doolan, K. R.; Mackie, J. C. *Combust. Flame* **1983**, *49*, 221.
- (10) Mackie, J. C.; Colket, M. B.; Nelson, P. F. *J. Phys. Chem.* **1990**, *94*, 4099.
- (11) (a) Terentis, A.; Doughty, A.; Mackie, J. C. *J. Phys. Chem.* **1992**, *96*, 10334. (b) Doughty, A.; Mackie, J. C. *J. Phys. Chem.* **1992**, *96*, 10339.
- (12) Chen, Y.; Rauk, A.; Tschuikow-Roux, E. *J. Chem. Phys.* **1991**, *94*, 7299.
- (13) Smith, M. BSc (Hons) Thesis, School of Chemistry, University of Sydney, 1998.
- (14) Glänzer, K.; Maier, M.; Troe, J. *J. Phys. Chem.* **1980**, *84*, 1681.
- (15) Dixon, D. A. *J. Phys. Chem.* **1986**, *90*, 54.
- (16) O'Gara, J. E.; Dailey, W. P. *J. Am. Chem. Soc.* **1992**, *114*, 3581.
- (17) Atkinson, B.; McKeagan, D. *J. Chem. Soc., Chem. Commun.* **1966**, 189.
- (18) Kee, R. J.; Miller, J. A.; Jefferson, T. H. *CHEMKIN; A General Purpose, Problem Independent, Transportable FORTRAN Chemical Kinetics*

Code Package, SANDIA National Laboratories Report SAN80-003; Sandia Laboratories: Albuquerque, NM, March, 1980.

(19) Mitchell, R. E.; Kee, R. J. *A General Purpose Computer Code for Predicting Chemical Kinetic Behavior Behind Incident and Reflected Shocks*; SANDIA National Laboratories Report SAND82-8205; Sandia Laboratories: Albuquerque, NM, March 1982.

(20) Hindmarsh, A. C. *LSODE and LSODI; Two New Initial Value Differential Equation Solvers*; ACM Signum Newsletter **1980**, 15, 4.

(21) Lutz, A. E.; Kee, R. J.; Miller, J. A. *SENKIN: A FORTRAN Program Predicting Homogeneous Gas-Phase Chemical Kinetics with Sensitivity Analysis*; SANDIA National Laboratories Report SAND87-8248; Sandia Laboratories: Albuquerque, NM, Feb. 1988.

(22) Pritchard, G. O.; Nilsson, W. B.; Kirtman, B. *Int. J. Chem. Kinet.* **1984**, 16, 1637.

(23) Poutsma, J. C.; Paulino, J. A.; Squires, R. R. *J. Phys. Chem. A* **1997**, 101, 5327.

(24) Mallard, W. G.; Westley, F.; Herron, J. T.; Hampson, R. F. *NIST*

Chemical Kinetic Database, Ver 6.0; NIST Standard Reference Data; NIST: Gaithersburg, MD, 1994.

(25) Schug, K. P.; Wagner, H. Gg.; Zabel, F. *Ber. Bunsen-Ges. Phys. Chem.* **1979**, 83, 167.

(26) Ainagos, A. F. *Kinet. Catal.* **1991**, 32, 720.

(27) Atkinson, B.; Atkinson, V. A. *J. Chem. Soc.* **1957**, 2086.

(28) Simmie, J. M.; Quiring, W. J.; Tschuikow-Roux, E. *J. Phys. Chem.* **1969**, 73, 3830.

(29) Atkinson, B.; Trenwith, A. B.; *J. Chem. Soc.* **1953**, 2082.

(30) Benson, S. W. *Thermochemical Kinetics*; John Wiley: New York, 1976.

(31) Bomse, D. S.; Berman, D. W.; Beauchamp, J. L. *J. Am. Chem. Soc.* **1981**, 103, 3967.

(32) McMillen, D. E.; Golden, D. M. *Annu. Rev. Phys. Chem.* **1982**, 33, 493.

(33) Hynes, R. G. Ph.D. Thesis, University of Sydney, 1998.